JOURNAL OF THERMOPHYSICS AND HEAT TRANSFER
Vol. 37, No. 2, April–June 2023

Experimental Study of Dynamic Ice Accretion Process over Rotating Aeroengine Fan Blades

Linchuan Tian,* Linkai Li,* Haiyang Hu,* and Hui Hu†
Iowa State University, Ames, Iowa 50011-2271

https://doi.org/10.2514/1.T6667

An experimental campaign was conducted to study dynamic ice accretion on rotating aeroengine fan blades and evaluate the icing-induced performance degradation to the fan rotor. The experiments were performed in an icing research tunnel with a scaled spinner-fan model exposed to typical dry rime and wet glaze icing conditions. Although the accreted ice layers were found to conform well with the shapes of the fan blades under the rime icing condition, the performance of the fan rotor was found to degrade substantially due to the much rougher blade surfaces, causing up to 60% reduction in the pressure increment after 360 s of the rime icing experiment. More complicated, needlelike icicles were found to grow rapidly over the rotating spinner and fan blades under the glaze icing condition due to the combined effects of the aerodynamic forces and the centrifugal forces associated with the rotation motion. The irregular-shaped glaze ice structures were found to induce tremendous detrimental effects on the fan rotor, making the airflow depressurized, instead of pressurized, after passing the iced fan rotor. The iced spinner-fan model was always found to consume more power, regardless of rime or glaze ice structures accreted on the fan blades.

Nomenclature

A_c	=	ice accumulation parameter
C	=	chord length at the midspan of the fan blade
$C_{\Delta P}$	=	pressure increment coefficient of the fan rotor
$C_{\Delta P\,\text{no-ice}}$	=	pressure increment coefficient for the case without ice accretion on fan blades
D_{fan}	=	outer diameter of fan rotor
D_{spinner}	=	base diameter of the elliptical-shaped spinner
J	=	advance ratio of the spinner-fan model
L_s	=	length of the elliptical-shaped spinner
l	=	the maximum thickness of the fan blade at the middle span.
M_{water}	=	water mass injected into Iowa State University's icing research tunnel for the icing experiment
N	=	number of fan blades
P	=	power input supplied to the electric model
P_{s1}	=	air pressure in the front of the fan rotor
P_{s2}	=	air pressure after passing the fan rotor
T_∞	=	temperature of the incoming airflow
t	=	ice accretion time
u, v, w	=	X, Y, and Z components of the flow velocity
V_∞	=	incoming airflow speed
X, Y, Z	=	Cartesian coordinate system
ΔP	=	airflow pressure increment across the fan rotor
η	=	mechanical efficiency of the electric motor
θ	=	blade trailing-edge thickness
ρ_{air}	=	density of the incoming airflow
ρ_{ice}	=	density of the ice
τ	=	required torque to drive the spinner-fan model.
Ω	=	rotation speed of the fan rotor

I. Introduction

ICING is one of the most serious hazards to aircraft flight in cold weather [1–4]. As an airplane flies in cold climate, supercooled airborne water droplets, which make up clouds and fog, impact and freeze on the exposed airframe surfaces to form ice shapes. Ice accretion may take place on every exposed frontal surface of an airplane: not only on the wings, propellers, and windshields [5,6] but also on the exposed surfaces of aeroengine components, such as inlet lips, fan spinners, rotor blades, and inlet guide vanes. Ice formation/accretion on rotating spinner and fan blades leads to an imbalanced compressor rotation, causing serious vibrations. The shedding of large ice chunks from engine inlet lips, spinners, or/and fan blades may also damage the fan rotor and other engine components, or even be sucked into the engine core, causing "power-loss" problems like stall, surge, and flameout [7]. Although extensive theoretic, numerical, and experimental studies have been conducted to examine aircraft icing phenomena in recent years, most of the previous studies focused on ice accretion on aircraft wings; only a limited number of studies can be found in the literature that examine aeroengine icing phenomena [8–15].

Fan blades are very important components of an aeroengine, which are designed not only to assist in sucking enough airflow into the engine core but also to compress the airflow (i.e., to increase the total pressure of the airflow across the fan rotor) for thrust generation [16,17]. In comparison to those on the surfaces of fixed aircraft wings, the dynamic ice accretion process on rotating fan blades becomes much more complicated due to the combined effects of aerodynamics shear forces exerted by the incoming airflow and the centrifugal forces associated with the rotation motion. A few numerical studies were performed in the past decades to investigate ice accretion on rotating fan blades. Das et al. [18,19] conducted numerical studies to investigate ice accretion on a high bypass turbofan engine booster rotor under different operating conditions. Hutchings [20] performed a numerical investigation on the shape changes of fan blades due to ice accumulation and evaluated the performance degradation induced by the ice accretion. It was found that, for a test case with the maximum ice accretion thickness being about 8% of the blade chord length, although the pressure loss was be tripled due to the ice accretion, the rate of the airflow inhaled by the fan rotor was reduced by up to 15%. Bidwell [21] used NASA's ice simulation package, LEWICE3D, to examine the icing issues on an energy efficient engine and found that supercooled water droplets with greater droplet sizes resulted in increased impingement rates on the engine's fan blades. Hamed et al. [22] also conducted a numerical study to examine the trajectories of water/ice droplets and the corresponding collection efficiency on rotating fan blades. They found that the water collection efficient (thereby, the ice accumulation on the fan blades) would be much greater for the case with larger water droplets. Dong et al. [23] also reported a numerical study to investigate ice accretion on

Presented as Paper 2022-2435 at the AIAA SciTech 2022 Forum, San Diego, CA, January 3–7, 2022; received 1 June 2022; revision received 14 August 2022; accepted for publication 22 September 2022; published online 31 October 2022.

*Postdoctoral Student, Department of Aerospace Engineering, Iowa State University.
†Martin C. Jischke Professor; huhui@iastate.edu. Associate Fellow AIAA.

rotating fan blades; the characteristics of the ice accretion on the blades were examined by comparing the shapes of the accreted ice layers at different spanwise positions. Although many important findings were revealed about the ice accretion process on engine fan blades, almost all the previous studies were performed based on numerical simulations. Comprehensive experimental studies are highly desirable to gain further insight into the underlying physics pertinent to aeroengine icing phenomena as well as to establish a comprehensive experimental database for the validation and verification of numerical simulations and aeroengine icing modeling, which are very essential for the development of more effective and robust anti-/deicing strategies to ensure safer and more efficient operation of aeroengines in cold weather.

In the present study, an experimental campaign was conducted to quantify the characteristics of the dynamic ice accretion process over the surfaces of rotating fan blades of an aeroengine model and to evaluate the detrimental effects of the ice accretion on the performance of the aeroengine fan rotor. The icing experiments were performed in an icing research tunnel (IRT) available at Iowa State University (ISU) with a scaled aeroengine spinner-fan model exposed to typical dry rime and wet glaze icing conditions. During the experiment, a high-resolution imaging system along with a phase-locking mechanism was used to acquire "phase-locked" snapshot images of the iced fan blades to reveal the important features of the dynamic ice accretion process. The pressure variations of the airflow before and after passing the fan rotor (i.e., in the term of the pressure increment coefficient of the fan rotor) and the required power input to drive the spinner-fan model to rotate at a constant angular speed (i.e., the power consumption data of the spinner-fan model) were also measured during the icing process. The time-resolved airflow pressure measurements and the power consumption characteristics were correlated with the acquired images of the iced fan blades to elucidate the underlying physics pertinent to aeroengine icing phenomena. To the best knowledge of the authors, the work reported here represents the first comprehensive experimental investigation to provide temporally resolved measurements to quantify the dynamic icing process over the surfaces of rotating fan blades and to characterize the detrimental effects of ice accretion on the performance of the spinner-fan model under different icing conditions.

II. Experimental Setup and Test Model

A. Brief Introduction of Icing Research Tunnel Used for Present Study

The experimental study was performed in the icing research tunnel of Iowa State University. As shown schematically in Fig. 1, the ISU's IRT has a transparent test section of 400 mm in width, 400 mm in height, and 2000 mm in length. It has a capacity of generating an airflow with a maximum wind speed (i.e., V_∞) of up to 60 m/s and a temperature (i.e., T_∞) down to −25°C. A water spray system, which consists of arrays of eight pneumatic atomizing spray nozzles (Spraying Systems Co., 1/8NPT-SU11), was installed at the entrance of the contraction section of the ISU's IRT to inject microsized water droplets into the test section. By adjusting the pressure regulators of the air and water supply lines connected to the atomizer/spray nozzles, the liquid water content (LWC) level of the airflow inside ISU's IRT can be controlled from 0.1 to 5.0 g/m^3. Based on the measurement results of a LaVision's ParticleMaster^{TM} system, the sizes of the water droplets exhausted from the atomizers/spray nozzles were found to range from 10 to 100 μm, with the corresponding mean volume diameter being about 20 μm. At the given testing conditions, the temperature distributions inside the test section of the ISU'S IRT were found to be quite uniform and stable, with the temperature fluctuations being less than 1.0°C, as measured by using thermocouple probes. In summary, the ISU'S IRT can be used to simulate atmospheric icing phenomena over a range of icing conditions (i.e., from very dry rime icing to extremely wet glaze icing conditions). By leveraging the ISU'S IRT, various studies have been conducted in recent years to study various atmospheric icing phenomena, including aircraft icing, wind turbine icing, stayed bridge cable icing, and power transmission cable icing [24–30].

B. Spinner-Fan Model Used in Present Study

A spinner-fan model was installed in the middle of the ISU'S IRT test section for the experimental campaign. The spinner-fan model was designed based on a Boeing 18 in. aeroengine test rig, as described by Ganz et al. [31], with a scale ratio of 1:2.3. Figure 1c shows the schematics of a fan blade used in the present study, which had a chord length of $C = 34$ mm at 50% of the blade midspan, a 0.402 hub/tip ratio, and a 1.65 in. aspect ratio. Eighteen fan blades

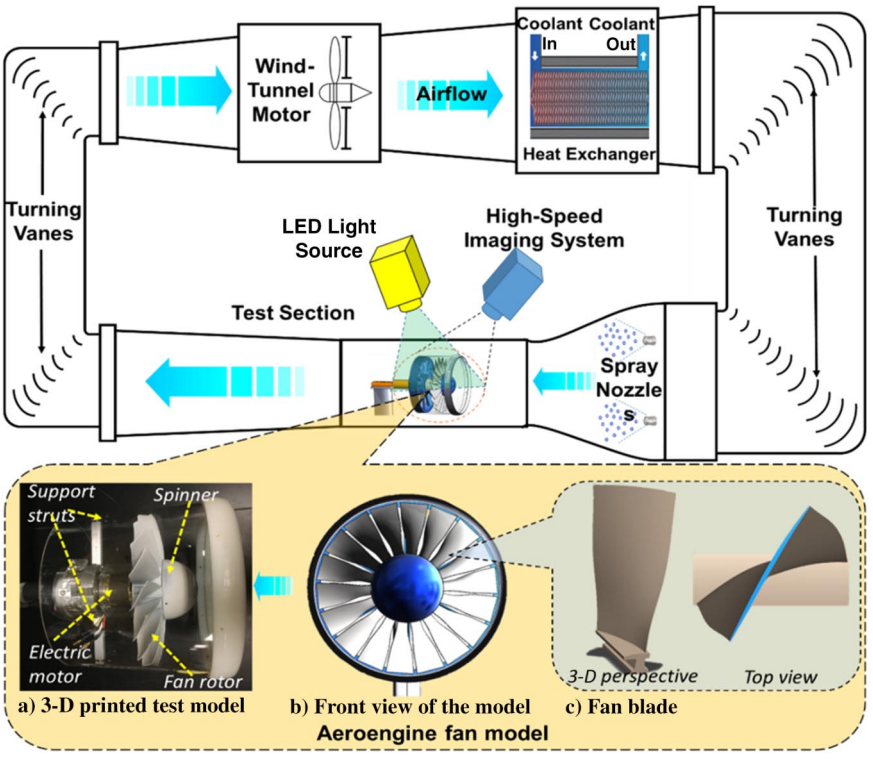

Fig. 1 Schematics of the ISU'S IRT and the test model used in the present study.

were mounted uniformly on a rotor disk, resulting in a tip solidity of 1.035 and a hub solidity of 2.214 for the fan rotor. An elliptical-shaped spinner with a maximum base diameter of $D_s = 80$ mm and a length of $L_s = 40$ mm was mounted in the front of the spinner-fan model to ensure smooth entrance of the airflow into the fan rotor. A cylindric plexiglass duct, a rounded lip ring, and four support struts were assembled to compose the nacelle of the spinner-fan model. The gap between the tips of the fan blades and the inner wall of the nacelle case was set to be 1.0 mm.

All the components of the spinner-fan model (except for the transparent, plexiglass nacelle case) were made of hard-plastic material (i.e., Stratasys, Inc.'s VeroWhitePlus) and manufactured by using a rapid prototyping machine [i.e., three-dimensional (3-D) printer] that built the parts layer by layer with a resolution of about 25 μm. The external surfaces of the fan blades and the elliptical spinner were further polished with fine sandpaper (i.e., up to 2000 grit) to achieve a very smooth, glossy finish. The primary design parameters of the spinner-fan model are summarized in Table 1.

In the present study, a direct current power supply (B&K Precision's 1692) was used to power the brushless motor (Scorpion's SII-4020-420 KV), which was connected to the rotor disk of the spinner-fan model. A proportional–integral–derivative feedback control module (Scorpion Commander's 15 V 60 A ESC) along with a data acquisition system (National Instruments USB-6218) and a LabView platform were used to maintain the rotation speed of the spinner-fan model, rotating at a constant angular speed during the entire duration of the icing experiment.

C. Determination of Controlling Parameters Used for Icing Experiments

A kinematic similarity is used to determine the operation parameters of the spinner-fan model used in the present study to simulate the ice accretion process on the rotating fan blades of a typical commercial aeroengine (e.g., a CFM56-2/3 engine). More specifically, the kinematic similarity is applied by using the same value of a dimensionless parameter (called the advance ratio or rotation factor) to examine the effects of the rotation motion on the dynamic ice accretion process over the surfaces of the fan blades. As described by Zhang et al. [32], the advance ratio J is defined as the velocity ratio of the incoming airflow velocity to the moving speed at the fan tip, which is expressed as $J = V_\infty/(\pi \cdot \Omega \cdot D_{\text{fan}})$, where V_∞ is the incoming flow speed, Ω is the rotation speed, and D_{fan} is the outer diameter of the spinner-fan model.

The CFM56-2/3 turbofan aeroengine is used as the design reference to determine the advance ratio of the spinner-fan model for the icing experiments. The CFM56-2/3 aeroengine has an advance ratio of 1.8 (i.e., $J = 1.8$) at the cruise condition, according to the datasheet released from European Aviation Safety Agency [33]. To match this advance ratio, the rotation speed of the spinner-fan models used in the present study was kept constant rotation at $\Omega = 2500$ rpm during the icing experiments and the incoming airflow velocity was set at $V_\infty = 15$ m/s. Table 2 gives a comparison of the relevant parameters of the CFM56-2/3 engine and the spinner-fan models used in the present study.

As described in Federal Aviation Administration's (FAA's) Airworthiness Standard of Title 14 of the Code of Federal Regulations (CFR) via Part 25 [34] or Part 33 [35,36], the in-flight icing conditions, which are used to guide ice protection systems design for airframe or aeroengines, are defined in Title 14 of Part 25 of the CFR in Appendix C and Appendix O (Super-Cooled Large Drop Icing Conditions). Although continuous maximum conditions are usually applied to airframe ice protection, intermittent maximum conditions are commonly referred to in the ice protection system design for aeroengines [37]. Therefore, the icing conditions used in the present study were selected based on the intermittent maximum envelope given in Part 25's Appendix C of the FAA's Title 14 of the CFR [34].

Table 1 Primary design parameters of the aeroengine spinner-fan unit models

Parameter	Value
Outer diameter of fan D_{fan}, mm	200
Spinner base diameter D_{spiner}, mm	80
Number of fan blades N	18
Blade trailing-edge thickness θ, mm	0.18
Blade hub-to-tip ratio	0.402
Blade aspect ratio	1.650
Blade tip thickness-to-chord ratio	0.025
Blade hub thickness-to-chord ratio	0.100

Table 2 Comparison of relevant parameters of CFM56-2/3 aeroengine and spinner-fan model used in the present study

Compared parameters	CFM 56-2/3 aeroengine	Spinner-fan model used in present study
Diameter of fan rotor D_{fan}, m	1.52	0.20
Maximum rotation speed $\Omega_{\max}$, rpm	5179	3000
Cruising speed V_∞, m/s	221.0	15.0
Cruising rotation speed, rpm	4900	2500
Temperature range T_∞, °C	≥ -40	≥ -15
Liquid water content, g/m^3	$0.1 \sim 3.0$	$0.1 \sim 3.0$
Advance ratio J	1.80	1.80

It is well known that in-flight ice accretion can be *rime*, *glaze*, or *mixed icing*, depending on the ambient conditions under which the icing event occurs [38–42]. When the ambient temperature is relatively low (i.e., typically below −8°C) and the airflow is relatively dry (i.e., having a lower LWC), supercooled water droplets carried by the incoming airflow freeze immediately upon impacting onto airframe surfaces, forming rime ice. At relatively warmer temperatures [i.e., just below the water freezing temperature (i.e., typically above −8°C)], with a relatively high LWC level in the incoming airflow, the impinged supercooled water droplets freeze partially, with the remaining impacted water mass running back along the airframe surface and being subsequently frozen into ice at further downstream locations, forming glaze ice with much more complex ice shapes. Mixed icing refers a situation with a simultaneous appearance or a combination of the rime and glaze ice characteristics. In the present study, although the speed of the incoming airflow in the ISU'S IRT was kept constant (i.e., $V_\infty = 15$ m/s) during the icing experiments, both the rime and glaze ice accretion processes over the surfaces of the rotating fan blades were investigated by changing the temperature and LWC levels in the incoming airflow. Table 3 summarizes the primary parameters used in the present study for the rime and glaze icing experiments.

As described by Anderson [43] and Waldman and Hu [44], the ice accumulation parameter is usually used to characterize the ice accretion process over an airfoil surface. Following up on the work of Anderson [43], the ice accumulation parameter A_c is defined as

$$A_c = \frac{\text{LWC} \cdot V_\infty \cdot t}{\rho_{\text{ice}} \cdot l} \tag{1}$$

where LWC refers to the liquid water content in the incoming airflow, V_∞ is the incoming airflow velocity, t is the ice accretion time, ρ_{ice} is the ice density, and l is the characteristic length of the airfoil (e.g., the maximum thickness of the blade in the present study). As given in Eq. (1), for the same incoming airflow velocity and the same spinner-fan model used in the present study, the value of the ice accumulation

Table 3 Primary parameters used for rime and glaze icing experiments

Icing type	Velocity of incoming airflow V_∞, m/s	Temperature of airflow T_∞, °C	Liquid water content in airflow, g/m^3
Rime icing	15.0	−15.0	0.50
Glaze icing	15.0	−5.0	2.0

parameter of A_C varies linearly with the LWC value and the ice accretion time t.

In the present study, each trial of the icing experiments was ended after a total amount of 1.0 kg of water mass (i.e., $M_{\text{water}} = 1.0$ kg) was sprayed into the ISU'S IRT. Because the LWC level in the incoming airflow for the rime icing case (i.e., LWC $= 0.50$ g/m^3) is much smaller than that of the glaze icing case (i.e., LWC $=$ 2.0 g/m^3), the duration of the rime icing experiments (i.e., total duration of ~600 s) was found to be 4.0 times the glaze icing experiments (i.e., total duration of ~150 s); the corresponding value of the ice accumulation parameter was found to be $A_c \approx 0.18$, as predicted theoretically by using Eq. (1).

It should also be noted that the research work presented here is a fundamental icing physics study with the primary objective to elucidate the underlying physics for a better understanding of aeroengine icing phenomena; the spinner-fan test model used in the present study is much simplified, and the icing experiments were conducted with a much lower incoming airflow speed in comparison to those of realistic aeroengines. Although the effects of the design/operation parameters of the fan blades for a specific aeroengine on the ice accretion process are beyond the scope of the present study, a parametric study will be conducted in the near future to characterize the effects of some important design/operation parameters of aeroengine fan blades (e.g., blade geometry, blade tip clearance, and materials of the fan blades and their working Mach number) on the dynamic ice accretion over the rotating fan blades.

D. Measurement Systems Used in Present Study

In the present study, a high-resolution imaging system (pco.dimax S4 camera with maximum 2016 × 2016 pixel resolution) along with a 50 mm macrolens (Nikon, 50 mm Nikkor 1.8D) were mounted above the ISU'S IRT test section to record the dynamic ice accretion process on the rotating fan blades. During the experiment, the rotation of the fan blades was monitored by using a digital tachometer (MONARCH, PLT200), which can generate one pulsed signal per rotation cycle. The pulsed signal was then used to trigger the imaging system for the phase-locked image acquisition to reveal the features of the ice accretion on the rotating fan blades more clearly. A pair of 200 W studio light-emitting diode (LED) lights (RPS Studio, model RS-5620) were used to provide low-flicker illumination to for the image acquisition. Based on the acquired ice accretion images, a comprehensive image processing procedure was used in the present study to extract quantitative information about the thickness profiles of the ice layers accreted along the leading edges (LEs) of the fan blades (i.e., LE ice thickness). The implemented image processing algorithms include Gaussian filtering for noise reduction, background removing, binary treatment for edge enhancing, and a Canny algorithm for edge detection [44,45]. Because the ice accreted on the fan blades is highly three-dimensional with complex topological features, the outlines of the ice layers extracted from the acquired images of the iced fan blades represent the outmost profiles of the ice layers accreted along the leading edges of the blades.

It is well known that one of the important functions for a fan rotor is to compress the airflow inhaled by the aeroengine (i.e., to increase total pressure of the airflow across the fan rotor) for thrust generation to augment the propulsion performance of the aeroengine. As shown schematically in Fig. 1, two rows of pressure taps were embedded on the nacelle of the spinner-fan model, which were used to measure the pressure changes of the airflow before (i.e., P_{s1}) and after (i.e., P_{s2}) passing the fan rotor during the icing experiment. The pressure taps were connected to a digital pressure sensor array (Scanivalve, DSA-3217), which has ±10 in. H_2O pressure range and ±0.2% static accuracy for the pressure measurements. The variations of the measured pressure increment across the fan rotor (i.e., $\Delta P = P_{S2} - P_{S1}$) were used to characterize the effects of the ice accretion over the fan blades on the performance of the fan rotor under different icing conditions.

During the icing experiments, the voltage applied to the electric motor and the current in the electric circuit were also monitored by using a multimeter and a current transducer (Crmagnetics, CR5410-50). The recorded electric current and applied voltage data were used to calculate the required power input supplied to the electric motor (i.e., power consumption) in order to maintain the aeroengine spinner-fan model rotating at the preset angular speed of $\Omega = 2500$ rpm during the icing experiments.

Before starting the icing experiments, the ISU'S IRT was operated at the prescribed frozen-cold temperature levels for at least 30 min without switching on the water spray system to ensure that the ISU'S IRT reached a thermal steady state. After turning on the water spray system, microsized water droplets exhausted from the spray atomizers/nozzles cooled down rapidly to become airborne, supercooled water droplets. The ice accretion process would start immediately as the airborne supercooled water droplets impinged onto the surfaces of the spinner-fan model. Although the ice accretion over the surface of the spinner was investigated systematically by Li et al. [12], the present study focuses on characterizing the dynamic ice accretion process over the rotating fan blades.

III. Measurement Results and Discussions

A. Acquired Phase-Locked Images Ice Accretion Process on Rotating Fan Blades

Figure 2 gives acquired phase-locked images to reveal the dynamic ice accretion process over the surfaces of rotating fan blades under the rime icing conditions of $V_\infty = 15$ m/s, $T_\infty = -15$°C, and LWC $= 0.50$ g/m^3. Similar to what was described by Liu and Hu [46], because the heat transfer process under such cold and dry icing conditions is sufficiently strong to remove/dissipate all the released latent heat of fusion associated with the solidification (i.e., icing) process, the supercooled water droplets were found to be frozen into ice immediately upon impinging onto the surfaces of the spinner and fan blades. Although the ice structures were found to accrete within narrow regions along the leading edges of the blades, the accreted ice layers were found to conform to the original profiles of the fan blades well in general. The ice layers were found to accrete mainly on the pressure-side surfaces without any traces of water runback being observed over the blade surfaces. As the icing experiment continues, while the thickness of the ice layers accreted on the blades was found to increase monotonically with more supercooled droplets impinging onto the fan blades, the surfaces of the iced fan blades became much rougher as the ice accretion time increased. Due to the existence of air bubbles/pockets trapped between the rime ice grains, the accreted ice structures were found to be opaque and have a milk-white appearance, i.e., exhibiting typical rime ice characteristics as described by Hansman and Kirby [47].

Figure 3 gives some of the typical LE ice thickness profiles extracted from the acquired ice accretion images along with a "zoomed-in" view of the rime ice structures accreted on a typical fan blade, which can be used to reveal the features of the rime ice accretion on the rotating fan blades more clearly and quantitatively. Although ice accretion was found to take place over the entire span of the fan blade, accreted ice structures were found to have much greater coverage in the outboard regions, especially near the blade tips, in comparison to those in the inboard regions (i.e., near the blade roots). The LE ice thickness profiles reveal quantitatively that the thickness of the ice layer accreted along the blade leading edge was found to grow continuously as the ice accretion time increased, as expected. Although the accreted ice layers were found to have the largest coverage near the blade tips, the LE ice thickness at the midspan of the fan blades was found to be much thicker than that near the blade tips. Sharp ice horn structures were found to grow rapidly near the blade roots (i.e., at the location of $y/S \approx 0.1$), as shown clearly in the zoomed-in view of the iced blades given in Fig. 3. The formation of the sharp ice horn structures near the blade roots is believed to be closely related to the trajectories of the airborne supercooled droplets flying over the elliptical-shaped spinner. As revealed clearly from the particle image velocimetry (PIV) measurement results of Li et al. [12], because the direct impingement limit of supercooled droplets was found to be located at the midspan of the elliptical-shaped spinner, the supercooled water droplets carried by the incoming airflow were pushed away from the root region of the elliptical-shaped spinner. Therefore, rime ice structures were found to accrete

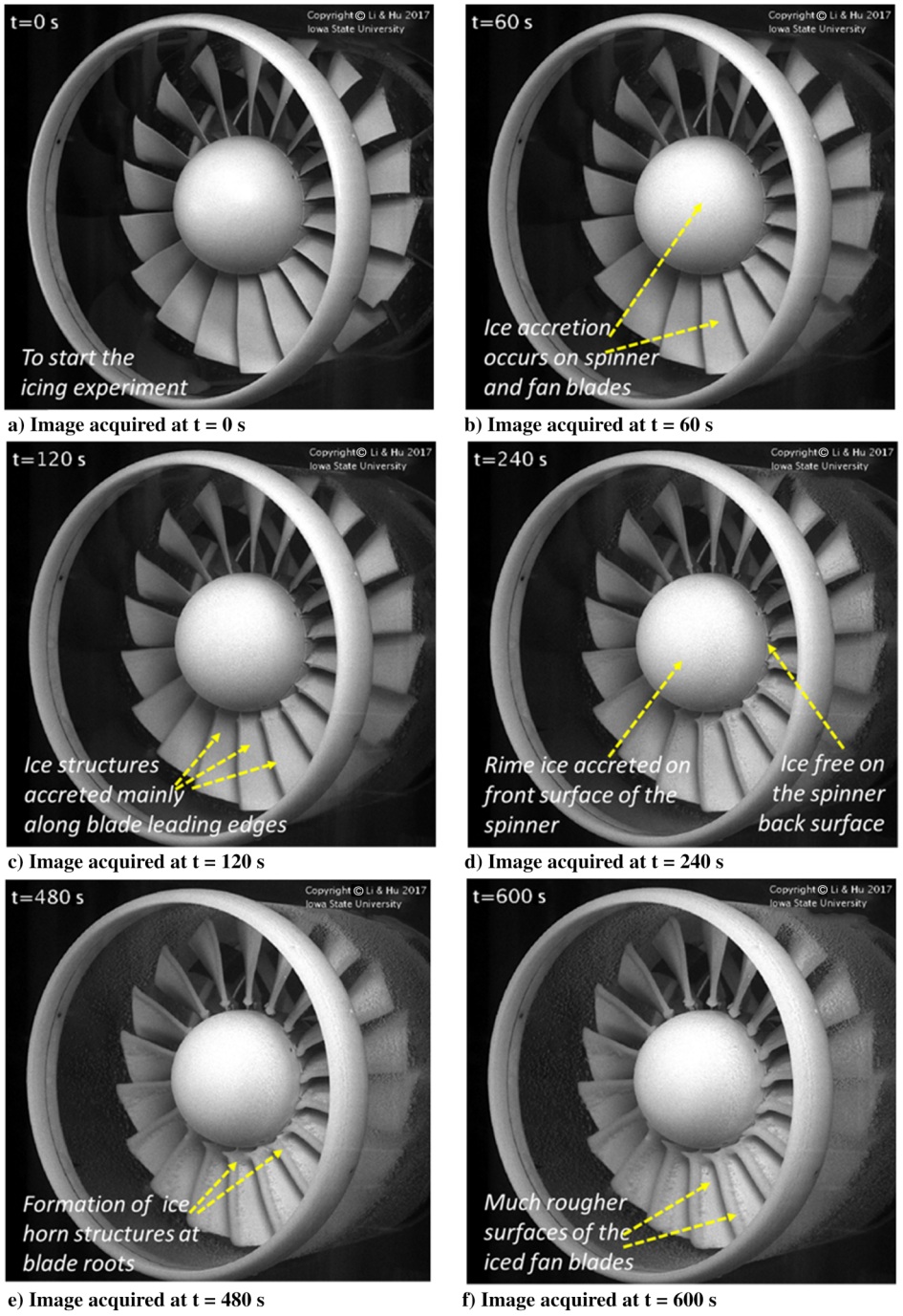

Fig. 2 Acquired phase-locked images to reveal the dynamic ice accretion on the rotating fan blades under the rime icing condition.

only over the front surface of the spinner, with the back surface near the fan blades being almost ice free, as revealed clearly in the acquired images given in Fig. 2. Therefore, as shown schematically in Fig. 3, instead of impinging onto the back surface of the elliptical-shaped spinner, the airborne water droplets flew over the spinner surface and impinged onto the surfaces of the downstream fan blades, subsequently causing the formation of sharp ice horn structures near the blade roots (i.e., at $y/S \approx 0.1$).

Figure 4 shows typical ice accretion images acquired during the glaze icing experiment under the testing condition of $V_\infty = 15$ m/s, $T_\infty = -5.0°$C, and LWC $= 2.0$ g/m^3. In comparison to the rime icing case described earlier in this paper, the characteristics of the glaze icing process over the surfaces of the rotating spinner and the fan blades were found to become much more complicated. Corresponding to the higher LWC level in the incoming airflow, much more supercooled water droplets (i.e., by a factor of four) would impinge onto the spinner and fan blades within the same time duration of the icing experiment, causing a significant amount of the latent heat of fusion released over the ice accreting surfaces of the spinner and fan blades. However, because the heat transfer process (i.e., both heat convection and conduction) became much weaker due to the warmer ambient temperature under the glaze icing condition (i.e., $T_\infty = -5.0°$C), the released latent heat of fusion could not be removed/dissipated rapidly from the ice accreting surfaces. As a result, only a portion of the impacted supercooled water droplets were frozen into ice right away, whereas the rest of the impinged water mass was found to remain in liquid over the surfaces of the spinner and fan blades.

Similar to what was described by Li et al. [12], the unfrozen water mass accumulated over the surface of the spinner would run back from the spinner nose to the spinner root, as driven by the aerodynamic shear force exerted by the incoming airflow. Meanwhile,

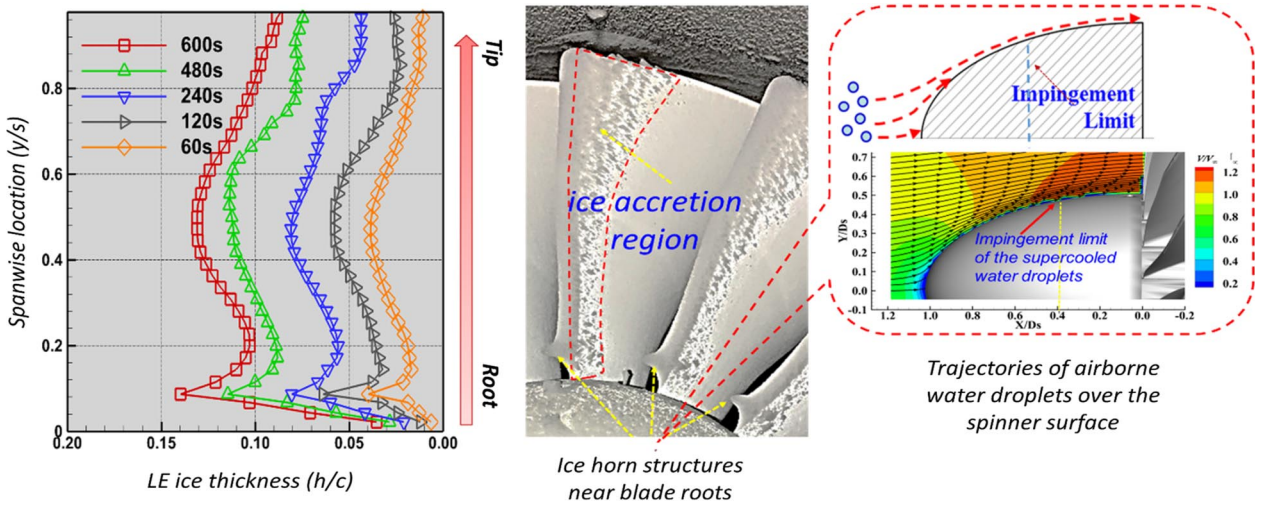

Fig. 3 Measured outer profiles of the ice layers accreted along the blade leading edges under the rime icing condition.

because of the centrifugal force associated with the rotation motion, a portion of the runback water would take off from the spinner surface and then subsequently freeze into ice, resulting in the formation of very complicated, needlelike icicles on the spinner surface, as shown clearly in Fig. 4 at $t \geq 60$ s. The needlelike icicles were found to grow outward rapidly and extrude further into the incoming airflow, which would catch more airborne water droplets to further accelerate the growth of the icicle structures. It should be noted that the formation of needlelike ice structures on the rotating spinner was also found in an actual inflight icing event of an aeroengine on an A321 aircraft after flying through freezing rain, and the acquired photographs were reported.[‡] As revealed clearly from the PIV measurement results given by Li et al. [12], the irregular-shaped glaze ice structures growing over the spinner surface induced great disturbances to the airflow around the spinner surface, causing significant changes to the flying trajectories of airborne water droplets above the spinner surface, thereby affecting the ice accretion process on the surfaces of the downstream fan blades.

Similar to the rime icing experiment, the impingement of the airborne supercooled water droplets was found to concentrate within narrow regions along the leading edges of the fan blades (i.e., within the direct impinging zones of the supercooled water droplets). Although only of a portion of the impacted water droplets was frozen into ice immediately under the glaze icing condition, the remaining unfrozen water was able to flow freely over the ice accreting blade surfaces. Although the aerodynamic shear forces exerted by the incoming airflow pushed the unfrozen water to run back along the blade surfaces to reach further downstream locations (i.e., running into further downstream regions beyond the direct impinging zones of the supercooled water droplets), the centrifugal force associated with the rotation motion of the fan blades drove the unfrozen water to move radially (i.e., transported the impacted water from the blade root to the tip), resulting in a much wider ice coverage on the fan blades and the formation of more complicated ice structures (i.e., forming irregular-shaped ice humps and horns) along the leading edges of the fan blades. As shown clearly in Fig. 5, the glaze ice structures accreted on the spinner and fan blades were found to be transparent and have a glassy appearance with obvious traces of water runback, i.e., exhibited typical features of glaze ice accretion as described by Hansman and Kirby [47].

The thickness distributions of the glaze ice layers accreted along the leading edges of the fan blades (i.e., LE ice thickness) were also extracted from the acquired glaze ice accretion images. Figure 5 gives the extracted LE ice thickness profiles as a function of the ice accretion time. Although the glaze ice accretion on the rotating fan blades was found to vary significantly along the spanwise direction, the thickness of the accreted ice layers along the blade leading edges was found to increase rapidly from the blade roots to the midspans, and then it decreased gradually from the midspans to the blade tips.

The zoomed-in view of the iced fan blades given in Fig. 5 reveals the features of the glaze ice accretion on the rotating fan blades more clearly. As driven by the aerodynamic shear forces exerted by the incoming airflow, the unfrozen water on the fan blades was forced to run back along the blade surfaces and then subsequently frozen into ice, resulting in the formation of runback ice structures at the further downstream locations (i.e., beyond the direct impinging zones of the supercooled water droplets). As a result, the coverage of the glaze ice accretion on the fan blades (i.e., as highlighted by the red dashed lines in the zoomed-in view of the iced fan blade) was found to become about 30% greater than that of the rime icing case. Furthermore, because of the centrifugal force associated with the rotation motion of the fan blades, the unfrozen surface water on the fan blades would flow radially from the blade roots to the tips under the glaze icing condition. Therefore, the ice layers accreted along the blade leading edges in the outboard region (i.e., near the blade tips) were found to grow much faster than those at the inboard region (i.e., close to the blade roots). Meanwhile, due to the strong effects of the centrifugal forces, a portion of the unfrozen water was even found to take off from the blade surfaces to form complex needle-shaped icicle structures extruding outward into the incoming airflow, as shown clearly in the zoomed-in view of the iced fan blades given in Fig. 5. Needle-shaped icicle structures were also observed to form at the blade tips due to the strong centrifugal forces in the blade tip regions.

Unlike the formation of sharp ice horn structures near the blade roots under the rime icing conditions, the glaze ice layers accreted near the blade roots were found to become much smoother with the accreted LE ice thickness, increasing monotonically from the blade root to midspan. The significant changes of the ice accretion characteristics in the regions near the blade roots are believed to be closely related to the formation of the complex needlelike icicles on the elliptical-shaped spinner under the glaze icing condition. The fast growth of the needlelike icicles over the spinner surface intercepted the incoming airborne water droplets in the region near the blade roots, resulting in less water droplets impacting onto the blade roots. Furthermore, even for the scenario in which airborne water droplets were not intercepted by the icicles accreted on the spinner surface, because only a portion of the impacted water mass was frozen into ice immediately upon impacting onto the blade surfaces, the centrifugal force associated with the rotation motion of the fan blades drove the unfrozen water to flow radially away from the blade roots. Therefore, the growth rate of the glaze ice layers in the region near the blade roots was found to be much slower in comparison to that of the rime icing case.

[‡]Data available online at https://blogtuan.info/2022/05/13/how-do-jet-engines-work-in-heavy-rain-and-ice-3/ [retrieved 8 October 2022].

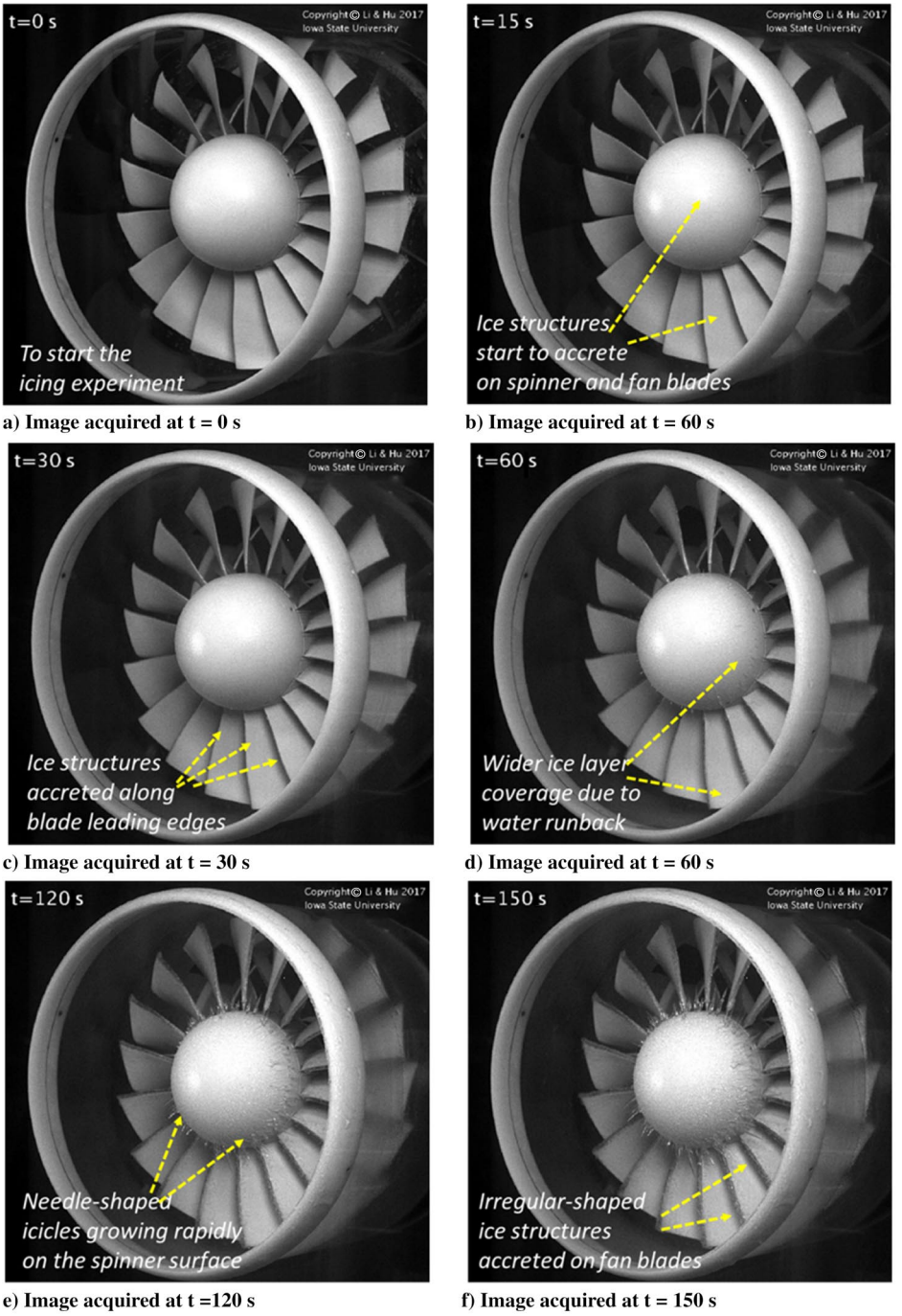

a) Image acquired at t = 0 s
b) Image acquired at t = 60 s
c) Image acquired at t = 30 s
d) Image acquired at t = 60 s
e) Image acquired at t =120 s
f) Image acquired at t = 150 s

Fig. 4 Acquired phase-locked images to reveal the dynamic ice accretion on the rotating fan blades under the glaze icing condition.

B. Characterizing Effects of Ice Accretion on Performance of Fan Rotor

It is well known that the fan rotor of an aeroengine is designed to increase the total pressure of the airflow inhaled by the aeroengine. A higher increment for the airflow pressure across the fan rotor would not only result in a greater thrust generated by the bypass airstream but also contribute to a higher compression ratio of the engine core, and thereby a higher combustion efficiency of the engine. In the present study, the effects of the ice accretion on the performance of the fan rotor were also evaluated by characterizing the pressure increments of the airflow across the fan rotor under different icing conditions. During the icing experiments, while the spinner-fan model was set to rotate at the constant angular speed of ($\Omega = 2500$ rpm, the variations of the airflow pressures across the fan rotor were measured by using pressure transducers connected to the pressure taps located before and after the fan rotor, as shown schematically in Fig. 1.

In the present study, a nondimensional parameter, named the pressure increment coefficient, is introduced to characterize the performance of the spinner-fan model, which is defined as

$$C_{\Delta P} = \frac{\Delta p}{q} = \frac{P_{S2} - P_{S1}}{\frac{1}{2}\rho_{\text{air}} V_\infty^2} \tag{2}$$

where P_{S1} and P_{S2} are the measured static pressure before and after the fan rotor, and V_∞ and ρ_{air} are the velocity and density of the incoming airflow. As the fan rotor operates properly under a normal condition (i.e., without ice accretion), the value of the pressure increment coefficient is expected to be positive (i.e., $C_{\Delta P} > 0$) because the fan rotor is designed to compress the airflow inhaled by the aeroengine, i.e., to make the air pressure after passing the fan rotor become greater than that upstream of the fan rotor (i.e., $P_{s2} > P_{s1}$). A greater pressure increment coefficient for the same spinner-fan model would indicate a higher-pressure increase for the

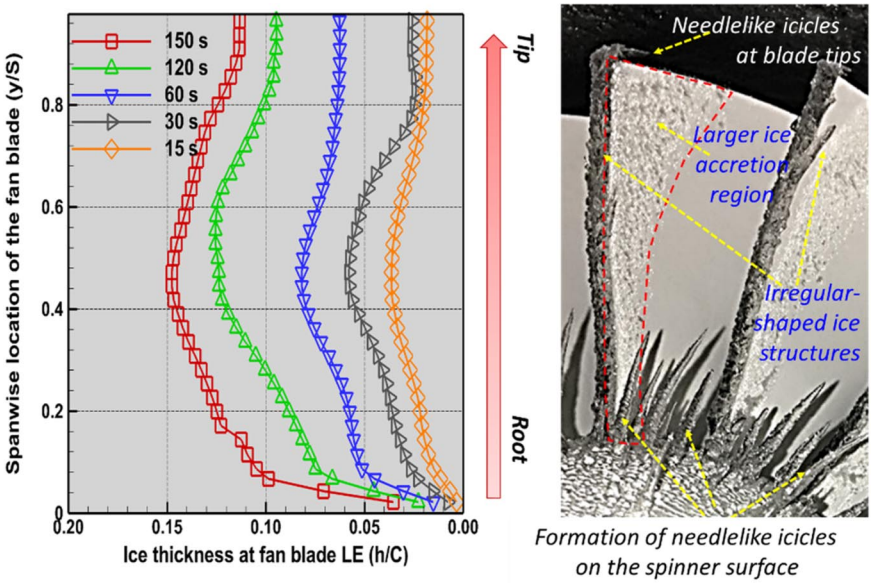

Fig. 5 Measured outer profiles of the ice layer accreted along the blade leading edges under the glaze icing condition.

airflow, resulting in a greater thrust generated by the bypass airstream as well as a higher compression ratio for the engine core compressor, and thereby a better thermodynamic efficiency of the engine.

To better illustrate the effects of the ice accretion on the performance of the spinner-fan model used in the present study, the pressure increment coefficients measured during the icing experiments were normalized by the corresponding value without any ice accretion (i.e., $C_{\Delta P}/C_{\Delta P\_\text{no-ice}}$), where $C_{\Delta P\_\text{no-ice}}$ is the pressure increment coefficient of the "clean" spinner-fan model measured before starting the icing experiment. It should be noted that the pressure increment coefficient of the clean spinner-fan model was found to be about 0.11 (i.e., $C_{\Delta P\_\text{no-ice}} \approx 0.11$) with the experimental settings used in the present study.

Figure 6 shows the measured pressure increment coefficient as a function of the ice accretion time. It can be seen clearly that the measured pressure increment coefficient of the spinner-fan model was found to increase gradually at the early stage of the rime icing process, reaching the peak value at the time of $t \approx 90$ s and then decreasing monotonically at the later stage of the rime icing experiment. Such an experimental observation was closely related to the characteristics of the rime icing process on the rotating spinner and fan blades. As described earlier in this paper, upon impacting onto the surfaces of the spinner and fan blades, supercooled water droplets carried by the incoming airflow were found to be frozen into ice instantly under the rime icing condition. The formation of rime ice grains over the front surfaces of the spinner and along the leading edges of the fan blades would make the surfaces becoming much rougher in comparison to the original surfaces with any ice accretion. Similar to what was reported by Shin [48], the ice roughness accreted at the initial stage of the rime icing process would act as a "turbulator" to promote fast transition of the laminar boundary-layer airflows over the fan blades, resulting in the improved aerodynamic performance of the spinner-fan model. Furthermore, because the rime ice layers accreted at the leading edges of the fan blades could follow the original profiles of the fan blades, the effective chord lengths of the rotating fan blades were extended due to the rime ice accretion, resulting in greater lift forces acting on the iced fan blades, i.e., a more effective compression of the fan rotor to the airflow. As a result, the pressure increment coefficient of the spinner-fan model was found to increase gradually (i.e., up to 10% increase) at the early stage of the rime icing process, as shown clearly in Fig. 6a.

However, with more and more supercooled water droplets impinging onto the spinner-fan model, the surfaces of the iced spinner and fan blades were also found to become rougher and rougher. As shown clearly in the zoomed-in view of the iced fan blades given in Fig. 3, complex, featherlike ice structures were found to accrete over the surfaces of the fan blades. The featherlike ice structures were found to grow against the incoming airflow, which would induce separation of the airflow from the fan blades, causing substantial aerodynamic

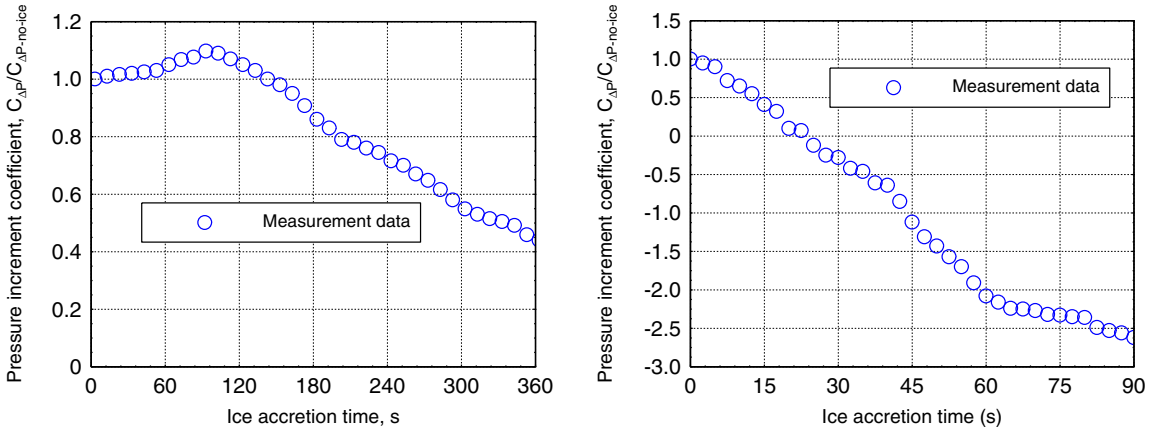

a) Under the rime icing condition **b) Under the glaze icing condition**

Fig. 6 Variations of the airflow pressure increment coefficient of the spinner-fan model as a function of the ice accretion time under different icing conditions.

performance degradation to the fan blades. As a result, the pressure increment coefficient of the spinner-fan model was found to decrease monotonically with the increasing ice accretion time at the later stage of the rime icing experiments (i.e., at $t > 90$ s). More specifically, as shown quantitatively in Fig. 6a, the pressure increment coefficient was found to become only 42% of its original value after 360 s of the rime icing experiment.

The variation characteristics of the measured pressure increment coefficient of the spinner-fan model under the glaze icing condition were found to become quite different from those under the rime icing condition. As shown clearly in Fig. 6b, whereas the measured pressure increment coefficients were found to decrease rapidly with the increasing ice accretion time under the glaze icing condition, the value of the measured pressure increment coefficient was even found to become negative about 20 s after starting the glaze icing experiment. Such variation features correlated well with the characteristics of the glaze icing process taking place on the spinner-fan model. As described earlier in this paper, because only a portion of the impacted supercooled water droplets were frozen into ice immediately under the glaze icing condition, the rest of the impacted water mass would stay in liquid over the surfaces of the spinner and fan blades. Due to the combined effects of aerodynamic shear force exerted by the incoming airflow and the centrifugal force associated with the rotation motion, the unfrozen water was found to run back and even take off from the surfaces of the rotating spinner and fan blades, resulting in the formation of complex irregular-shaped icicles extruding out from the surfaces of the rotating spinner and fan blades. As revealed clearly from the PIV measurements given by Li et al. [12], the irregular-shaped icicle structures accreted over the spinner surfaces induced large-scale airflow separations, which significantly degraded the quality of the airflow inhaled by the aeroengine (i.e., causing nonuniformity and increasing turbulence intensity levels of the airflow). Furthermore, the irregular-shaped glaze ice structures accreted along the leading edges of the rotating fan blades would not only induce massive airflow separations to degrade the aerodynamic performance of the fan blades significantly but also block the flowing passage of the airstreams to be inhaled by the aeroengine. All of these factors induced significant detrimental effects on the performance of the spinner-fan model. Therefore, the measured pressure increment coefficient of the spinner-fan model was found to decrease monotonically with the increasing ice accretion time under the glaze icing condition. As shown quantitatively in Fig. 6b, the value of the measured pressure increment coefficient was found to become negative only about 20 s after starting the glaze icing experiment. It indicates that the complex glaze ice structures accreted on the rotating spinner and fan blades degraded the performance of the spinner-fan model so significantly that the fan rotor would not be able to compress the airflow anymore. Instead, the pressure of the airflow was found to decrease substantially after passing the fan rotor due to significant detrimental effects induced by the glaze ice accretion.

C. Power Consumption of Spinner-Fan Model During Icing Accretion Process

As described earlier in this paper, while the spinner-fan model was set to rotate at a constant angular speed of $\Omega = 2500$ rpm during the icing experiments, the power consumption characteristics of the spinner-fan model under different icing conditions were examined by measuring the power supplied to the electric motor to drive the spinner-fan model. The power consumption (PC) of the spinner-fan model can be estimated by using following equation:

$$\mathrm{PC} = \tau \cdot \Omega = P \cdot \eta \tag{3}$$

where Ω is the rotational speed, and τ is the required torque to drive the spinner-fan model. P is the power input supplied to the electric model, and η is the mechanical efficiency of the electric motor. Because the rotational speed of the spinner-fan model was set to be the same during the icing experiments, the efficiency of the electric motor η would be a constant in the present study.

In the present study, a nondimensional parameter, named the power consumption ratio, is introduced to reveal the effects of the ice accretion on the power consumption of the spinner-fan model more clearly. The power consumption ratio is defined as the measured power consumption values of the spinner-fan model during the icing experiment normalized by the corresponding value of the clean spinner-fan model measured before starting the icing experiment (i.e., the value without any ice accretion), which is expressed as

$$\text{PC ratio} = \frac{\mathrm{PC_{ice}}}{\mathrm{PC_{no\text{-}ice}}} = \frac{\tau_{\mathrm{ice}}\Omega}{\tau_{\text{no-ice}}\Omega} = \frac{P_{\mathrm{ice}}}{P_{\text{no-ice}}} \tag{4}$$

Figure 7 gives the measured power consumption ratio values of the spinner-fan model under different icing conditions. Because ice accretion on the rotating spinner and fan blades not only induced greater aerodynamic drag forces due to the rougher surfaces for the iced spinner and fan blades but also caused an increased moment of inertia for the iced spinner-fan model, the required torque to drive the spinner-fan model rotating at the same rotational speed was expected to increase in general. As a result, the value of the power consumption ratio was found to always be greater than 1.0, as shown quantitatively in Fig. 7.

The measurement results given in Fig. 7a reveal clearly that, because the initial rime ice accretion was found to conform well with the original profiles of the spinner and fan blades in general, the power consumption of the spinner-fan model was found to increase only slightly at the initial stage of the rime ice accretion process (i.e., $t < 30$). Because the rime ice accreted along the leading edge of the fan blades became aerodynamically favorable at the early stage of the rime icing process, the fan blades were found to be able to compress airflow more effectively (i.e., add more energy into the airflow to increase the airflow pressure), as indicated by the increased pressure

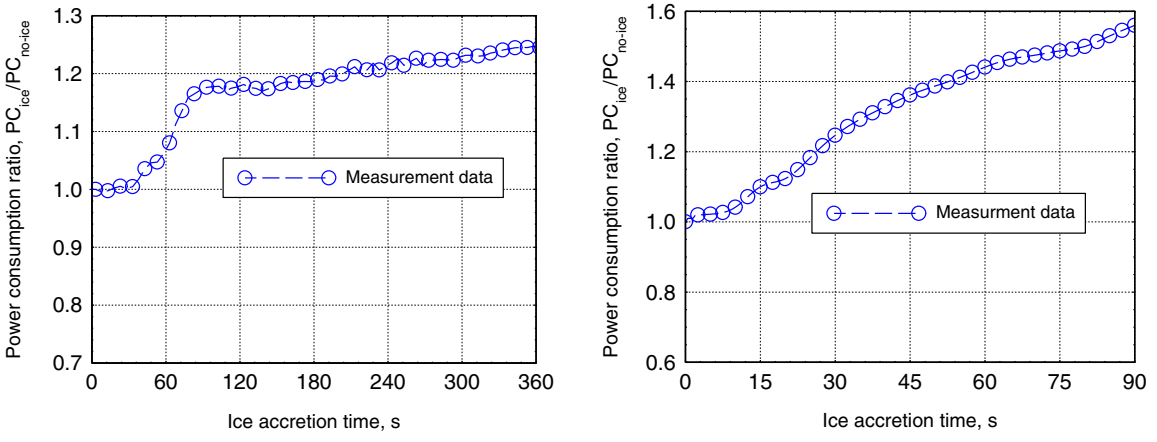

a) Underthe rime icing condition **b) Under the glaze icing condition**

Fig. 7 Power consumption characteristics of the spinner-fan model as a function of the ice accretion time under different icing conditions.

increment coefficient during the period of 30 s < t < 90 s, shown in Fig. 6a. Correspondingly, the power consumption of the spinner-fan model was found to increase rapidly during the period of 30 s < t < 90 s to balance the required extra power used for the airflow compression. At the later stage of the rime icing process, while the growth of irregular, featherlike rime ice structures over the blade surfaces induced large-scale flow separations and caused greater disturbances to the airflow, the increased surface roughness due to the thicker rime ice accretion also resulted in greater drag forces as the airstreams flowing over the iced spinner and fan blades. Therefore, whereas the pressure increment coefficient of the spinner-fan model decreased continuously at the later stage of the rime icing process, the power consumption value of the iced spinner-fan model was found to increase gradually due to the detrimental effects induced by the ice accretion. More specifically, after 360 s of the rime icing experiments, although the measured pressure increment coefficient was found to become only 42% of its original value, the power consumption of the iced spinner-fan model was found to increase about 25% in comparison to the corresponding value of the clean spinner-fan model.

As described earlier in this paper, the glaze icing process was found to become much more complicated due to the existence of the unfrozen impacted water over the surfaces of the rotating spinner and fan blades. As a result of the combined effects of the aerodynamic shear force and the centrifugal force, very complex irregular-shaped icicle structures were found to accrete over the surfaces of the rotating spinner and blade surfaces. The rapid growth of the irregular-shaped icicle structures induced massive flow separations over the surfaces of the rotating spinner and fan blades, degrading the aerodynamic performance of the spinner-fan model dramatically. As a result, much more power input was required to overcome the significantly greater aerodynamic drags acting on the iced spinner and fan blades during the glaze icing process. Therefore, the power consumption of the spinner-fan model was found to increase much more rapidly as the ice accretion time increased, as shown in Fig. 7b. More specifically, after only 90 s of the glaze icing experiment, the power consumption of the spinner-fan model was found to increase by about 58% in comparison to the corresponding value measured before starting the glaze icing experiment.

Based on the comparison of the power consumption data under different icing conditions, it can also be seen that, after spraying the same amount of the water mass into the test section of the ISU'S IRT, the power consumption of the spinner-fan model due to the glaze ice accretion was found to be about 2.3 times that required under the rime icing condition. It indicates that glaze ice accretion would induce much more serious detrimental effects on the performance of the spinner-fan model due to the formation of more complicated ice structures on the rotating spinner and fan blades. The more serious detrimental effects induced by the glaze ice accretion were found to agree well with the research findings reported by Liu et al. [28] when examining the ice accretion effects on the performance of rotating propeller blades.

IV. Conclusions

The present experimental study was conducted to investigate the dynamic ice accretion process on the surfaces of rotating aeroengine fan blades and to evaluate the detrimental effects of the ice accretion on the aerodynamic performance of the fan rotor. The icing experiments were performed in the icing research tunnel of Iowa State University with a scaled spinner-fan model that was exposed to typical dry rime and wet glaze icing conditions. During the icing experiments, while a high-speed imaging system was used to acquire phase-locked images to reveal the transient features of the dynamic ice accretion process over the surfaces of the rotating fan blades, both the pressure increments of the airflow before and after passing the fan rotor and the required power inputs supplied to drive the spinner-fan model to rotate at the same angular speed were measured quantitatively during the ice accretion process.

It was found that, whereas the ice accretion on the fan blades was concentrated within narrow bands along the blade leading edges under the dry rime icing condition, the accreted rime ice layers conformed well with the original profiles of the fan blades in general. Interestingly, the initial accretion of the rime ice structures was found to be aerodynamically favorable to cause a higher pressure of airflow across the fan rotor at the early stage of the rime icing process in comparison to the clean spinner-fan model without any ice accretion. However, with the surfaces of the iced fan blades becoming rougher and rougher at the later stage of the rime icing process, complicated, featherlike ice structures were found to grow outward from the blade surfaces to induce large-scale airflow separations over the blade surfaces, degrading the aerodynamic performance of the fan rotor substantially. As a result, whereas the pressure of the airflow across the fan rotor was found to decrease continuously with the increasing ice accretion time, the power consumption of the iced spinner-fan model was found to increase monotonically. More specifically, after 360 s of the rime icing experiment, whereas the pressure increment of the airflow across the iced fan rotor was found to decrease up to 60%, the power consumption of the spinner-fan model was found to increase about 25% in comparison with the corresponding values of the clean spinner-fan model without any ice accretion.

The characteristics of the dynamic ice accretion process on the rotating fan blades were found to become much more complicated under the wet glaze icing condition due to the existence of unfrozen impacted water over the blade surfaces. With the combined effects of the aerodynamic shear forces exerted by the incoming airflow and the centrifugal force associated with the rotation motion, the unfrozen surface water was found to run back to further downstream locations and flow radially from the blade roots to the tips. In comparison with the rime icing scenario, although the accreted glaze ice layers were found to have much wider coverage on the fan blades, much more complicated, needlelike icicle structures were observed to grow rapidly along the blade leading edges, inducing significant detrimental effects on the performance of the fan rotor. As a result, the airflow was found to be depressurized, instead of compressed, after passing the iced fan rotor. The power consumption of the spinner-fan model was also found to increase rapidly due to the glaze ice accretion. More specifically, after a short duration of 90 s of the glaze icing experiment, whereas the designed function of the fan rotor for airflow compression was ruined completely due to the glaze ice accretion, the power consumption of the iced spinner-fan model was found to increase by about 60% in comparison with its original value measured before starting the glaze icing experiment.

Acknowledgments

The Iowa Space Grant Consortium Base Program for Aircraft Icing Studies partially supported the research work. The support of National Science Foundation under award numbers CBET-1916380, CBET-1935363, and CMMI-1824840 is also gratefully acknowledged. The authors want to thank Yang Liu, James Benson, and Andrew Jordan of Iowa State University (ISU) for their help in operating the ISU's icing research tunnel Facility.

References

[1] Laforte, J. L., Louchez, P., Bouchard, G., and Ma, F., "A Facility to Evaluate Performance of Aircraft Ground de/Anti-Icing Fluids Subjected to Freezing Rain," *Cold Regions Science and Technology*, Vol. 18, No. 2, 1990, pp. 161–171. https://doi.org/10.1016/0165-232X(90)90005-H

[2] Huang, X., Tepylo, N., Pommier-Budinger, V., Budinger, M., Bonaccurso, E., Villedieu, P., and Bennani, L., "A Survey of Icephobic Coatings and Their Potential Use in a Hybrid Coating/Active Ice Protection System for Aerospace Applications," *Progress in Aerospace Sciences*, Vol. 105, 2019, pp. 74–97. https://doi.org/10.1016/j.paerosci.2019.01.002

[3] Cao, Y., Tan, W., and Wu, Z., "Aircraft Icing: An Ongoing Threat to Aviation Safety," *Aerospace Science and Technology*, Vol. 75, 2018, pp. 353–385. https://doi.org/10.1016/j.ast.2017.12.028

[4] Grishaev, V. G., Usachev, I. A., Drachev, V. P., Gattarov, R. K., Rudenko, N. I., Amirfazli, A., Borodulin, I. S., Bakulin, I. K., Makarov, M. V., and Akhatov, I. S., "Ice Imaging in Aircraft Anti-Icing Fluid Films Using

Polarized Light," *Cold Regions Science and Technology*, Vol. 194, 2022, Paper 103459.
https://doi.org/10.1016/J.COLDREGIONS.2021.103459

[5] Valarezo, W. O., Lynch, F. T., and McGhee, R. J., "Aerodynamic Performance Effects due to Small Leading-Edge Ice (Roughness) on Wings and Tails," *Journal of Aircraft*, Vol. 30, No. 6, 1993, pp. 807–812. https://doi.org/10.2514/3.46420

[6] Bragg, M. B., Gregorek, G. M., and Lee, J. D., "Airfoil Aerodynamics in Icing Conditions," *Journal of Aircraft*, Vol. 23, No. 1, 1986, pp. 1–12. https://doi.org/10.2514/3.45269

[7] Linke-Diesinger, A. *Systems of Commercial Turbofan Engines: An Introduction to Systems Functions*. Springer, Berlin, 2008.

[8] McGovern, R. K., Bulusu, K. V, Antar, M. A., and Lienhard, V. J. H., "One-Dimensional Model of an Optimal Ejector and Parametric Study of Ejector Efficiency," *Proceedings of the 25th International Conference on Efficiency, Cost, Optimization and Simulation of Energy Conversion Systems and Processes, ECOS 2012*, Vol. 2, 2012, pp. 303–313.

[9] Reddy, E. S., Abumeri, G. H., Murthy, P. L. N., and Chamis, C. C., "Structural Tailoring of Aircraft Engine Blade Subject to Ice Impact Constraints," *4th Symposium on Multidisciplinary Analysis and Optimization*, AIAA, Reston, VA, 1992, pp. 197–206; also AIAA Paper 1992-4710, 1992.
https://doi.org/10.2514/6.1992-4710

[10] Hamed, A., Das, K., and Basu, D., "Numerical Simulations of Ice Droplet Trajectories and Collection Efficiency on Aero- Engine Rotating Machinery," *43rd AIAA Aerospace Sciences Meeting and Exhibit*, AIAA, Reston, VA, 2005, pp. 1–10; also AIAA Paper 2005-1248, 2005.
https://doi.org/10.2514/6.2005-1248

[11] Li, L., Liu, Y., Tian, L., Hu, H., Hu, H., Liu, X., Hogate, I., and Kohli, A., "An Experimental Study on a Hot-Air-Based Anti-/de-Icing System for Aero-Engine Inlet Guide Vanes," *Applied Thermal Engineering*, Vol. 167, Aug. 2019, Paper 114778.
https://doi.org/10.1016/j.applthermaleng.2019.114778

[12] Li, L., Liu, Y., and Hu, H., "An Experimental Study on Dynamic Ice Accretion Process over the Surfaces of Rotating Aero-Engine Spinners," *Experimental Thermal and Fluid Science*, Vol. 109, 2019, Paper 109879.
https://doi.org/10.1016/J.EXPTHERMFLUSCI.2019.109879

[13] Al-Khalil, K. M., Keith, T. G., Dewitt, K. J., Nathman, J. K., and Dietrich, D. A., "Thermal Analysis of Engine Inlet Anti-Icing Systems," *Journal of Propulsion and Power*, Vol. 6, No. 5, 1990, pp. 1–9.
https://doi.org/10.2514/3.23264

[14] Lian, W., and Xuan, Y., "Experimental Investigation on a Novel Aero-Engine Nose Cone Anti-Icing System," *Applied Thermal Engineering*, Vol. 121, 2017, pp. 1011–1021.
https://doi.org/10.1016/j.applthermaleng.2017.04.160

[15] Lee, S., and Loth, E., "Simulation of Icing on a Cascade of Stator Blades," *Journal of Propulsion and Power*, Vol. 24, No. 6, 2008, pp. 1309–1316.
https://doi.org/10.2514/1.37810

[16] Yu, X.-J., and Liu, B.-J., "Stereoscopic PIV Measurement of Unsteady Flows in an Axial Compressor Stage," *Experimental Thermal and Fluid Science*, Vol. 31, No. 8, 2007, pp. 1049–1060.
https://doi.org/10.1016/j.expthermflusci.2006.11.001

[17] Yoon, J.-H., and Lee, S.-J., "Stereoscopic PIV Measurements of Flow Behind an Isolated Low-Speed Axial-Fan," *Experimental Thermal and Fluid Science*, Vol. 28, No. 8, 2004, pp. 791–802.
https://doi.org/10.1016/j.expthermflusci.2003.10.004

[18] Das, K., Hamed, A., Basu, D., and Mechanics, E., "Ice Shape Prediction for Turbofan Rotating Blades," *44th AIAA Aerospace Sciences Meeting and Exhibit*, AIAA, Reston, VA, 2006, pp. 1–12; also AIAA Paper 2006-0209, 2006.

[19] Das, K., "Numerical Simulations of Icing in Turbomachinery," Ph.D. Thesis, Univ. of Cincinnati, Cincinnati, OH, 2006.

[20] Hutchings, R., "Effects of Supercooled Water Ingestion on Engine Performance," M.S. Thesis, Univ. of Tennessee, Knoxville, Tennessee, 2011.

[21] Bidwell, C. S., "Particle Trajectory and Icing Analysis of the E 3 Turbofan Engine Using LEWICE3D Version 3," *4th AIAA Atmospheric and Space Environments Conference*, AIAA Paper 2012-3037, 2012.
https://doi.org/10.4271/2011-38-0048

[22] Hamed, A., Das, K., and Basu, D., "Numerical Simulations of Ice Droplet Trajectories and Collection Efficiency on Aero-Engine Rotating Machinery," AIAA, Reston, VA, Jan. 2012, pp. 1–10; also AIAA Paper 2005-1248, 2012.
https://doi.org/10.2514/6.2005-1248

[23] Dong, W., Zhu, J. J., Wang, R., and Chen, Y., "Numerical Simulation of Icing on the Rotating Blade," *Proceedings of the ASME Turbo Expo 2015: Turbine Technical Conference and Exposition*, American Soc. of Mechanical Engineers, Fairfield, NJ, 2015, pp. 1–9.

[24] Gao, L., Liu, Y., and Hu, H., "An Experimental Investigation on the Dynamic Glaze Ice Accretion Process over a Wind Turbine Airfoil Surface," *International Journal of Heat and Mass Transfer*, Vol. 149, 2020, Paper 119120.
https://doi.org/10.1016/J.IJHEATMASSTRANSFER.2019.119120

[25] Liu, Y., Ma, L., Wang, W., Kota, A. K., and Hu, H., "An Experimental Study on Soft PDMS Materials for Aircraft Icing Mitigation," *Applied Surface Science*, Vol. 447, 2018, pp. 599–609.
https://doi.org/10.1016/j.apsusc.2018.04.032

[26] Li, L., Liu, Y., Tian, L., Hu, H., Hu, H., Liu, X., Hogate, I., and Kohli, A., "An Experimental Study on a Hot-Air-Based Anti-/de-Icing System for Aero-Engine Inlet Guide Vanes," *Applied Thermal Engineering*, Vol. 167, 2020, Paper 114778.
https://doi.org/10.1016/j.applthermaleng.2019.114778

[27] Peng, Y., Veerakumar, R., Zhang, Z., Hu, H., Liu, Y., He, X., and Hu, H., "An Experimental Study on Mitigating Dynamic Ice Accretion Process on Bridge Cables with a Superhydrophobic Coating," *Experimental Thermal and Fluid Science*, Vol. 132, 2022, Paper 110573.
https://doi.org/10.1016/J.EXPTHERMFLUSCI.2021.110573

[28] Liu, Y., Li, L., Chen, W., Tian, W., and Hu, H., "An Experimental Study on the Aerodynamic Performance Degradation of a UAS Propeller Model Induced by Ice Accretion Process," *Experimental Thermal and Fluid Science*, Vol. 102, Nov. 2018, pp. 101–112.
https://doi.org/10.1016/j.expthermflusci.2018.11.008

[29] Zhang, Z., Ma, L., Liu, Y., Ren, J., and Hu, H., "An Experimental Study of Rain Erosion Effects on a Hydro-/Ice-Phobic Coating Pertinent to Unmanned-Arial-System (UAS) Inflight Icing Mitigation," *Cold Regions Science and Technology*, Vol. 181, 2021, Paper 103196.
https://doi.org/10.1016/j.coldregions.2020.103196

[30] Veerakumar, R., Gao, L., Liu, Y., and Hu, H., "Dynamic Ice Accretion Process and Its Effects on the Aerodynamic Drag Characteristics of a Power Transmission Cable Model," *Cold Regions Science and Technology*, Vol. 169, 2020, Paper 102908.
https://doi.org/10.1016/j.coldregions.2019.102908

[31] Ganz, U. W., Joppa, P. D., Patten, T. J., and Scharpf, D. F., "Boeing 18-Inch Fan Rig Broadband Noise Test," NASA CR 1998-208704, 1998.

[32] Zhang, M., Zhang, L., and Liu, Z., "Preliminary Research on Rotating Icing Test Scaling Law," *Research Journal of Applied Sciences, Engineering and Technology*, Vol. 8, No. 6, 2014, pp. 803–810.
https://doi.org/10.19026/rjaset.8.1037

[33] EASA Type-Certificate Data Sheet CFM 56-2 and CFM 56-3, European Aviation Safety Agency, 2008, https://www.easa.europa.eu/en/downloads/7689/en.

[34] "Aeronautics and Space," Airworthiness Standards: Transport Category Airplanes, Pt. 25, Title 14, Code of Federal Regulations, Federal Aviation Administration, U.S. Dept. of Transportation, Oct. 2022.

[35] "Aircraft Engines," *Airworthiness Standards: Aircraft Engines,* Pt. 33, Title 14, Code of Federal Regulations, Federal Aviation Administration, U.S. Dept. of Transportation, Oct. 2022.

[36] Bin, Y., and Yanpei, Z., "Icing Certification of Civil Aircraft Engines," *Procedia Engineering*, Vol. 17, 2011, pp. 603–615.
https://doi.org/10.1016/j.proeng.2011.10.076

[37] Jeck, R. K., "Icing Design Envelopes (14 CFR Parts 25 and 29, Appendix C) Converted to a Distance-Based Format," Federal Aviation Administration, U.S. Dept. of Transportation Final Rept. AR-00/30, April 2002.

[38] Politovich, M. K., "Predicting Glaze or Rime Ice Growth on Airfoils," *Journal of Aircraft*, Vol. 37, No. 1, 2000, pp. 117–121.
https://doi.org/10.2514/2.2570

[39] Papadakis, M., Rachman, A., Wong, S., Yeong, H., and Bidwell, C. S., "Water Droplet Impingement on Simulated Glaze, Mixed, and Rime Ice Accretions," NASA TM 2007-213961, Oct. 2007.

[40] Liu, Y., Bond, L. J., and Hu, H., "Ultrasonic-Attenuation-Based Technique for Ice Characterization Pertinent to Aircraft Icing Phenomena," *AIAA Journal*, Vol. 55, No. 5, 2017, pp. 1–8.
https://doi.org/10.2514/1.J055500

[41] Makkonen, L., and Oleskiw, M. M., "Small-Scale Experiments on Rime Icing," *Cold Regions Science and Technology*, Vol. 25, No. 3, 1997, pp. 173–182.
https://doi.org/10.1016/S0165-232X(96)00010-9

[42] Mangini, D., Antonini, C., Marengo, M., and Amirfazli, A., "Runback Ice Formation Mechanism on Hydrophilic and Superhydrophobic Surfaces," *Cold Regions Science and Technology*, Vol. 109, 2015, pp. 53–60.
https://doi.org/10.1016/j.coldregions.2014.09.012

[43] Anderson, D., "Acceptable Tolerances for Matching Icing Similarity Parameters in Scaling Applications," *39th Aerospace Sciences Meeting and Exhibit*, AIAA Paper 2001-0832, 2001. https://doi.org/10.2514/6.2001-832

[44] Waldman, R. M., and Hu, H., "High-Speed Imaging to Quantify Transient Ice Accretion Process over an Airfoil," *Journal of Aircraft*, Vol. 53, No. 2, 2016, pp. 369–377. https://doi.org/10.2514/1.C033367

[45] Liu, Y., Li, L., Ning, Z., Tian, W., and Hu, H., "Experimental Investigation on the Dynamic Icing Process over a Rotating Propeller Model," *Journal of Propulsion and Power*, Vol. 34, No. 4, 2018, pp. 933–946. https://doi.org/10.2514/1.B36748

[46] Liu, Y., and Hu, H., "An Experimental Investigation on the Unsteady Heat Transfer Process over an Ice Accreting Airfoil Surface," *International Journal of Heat and Mass Transfer*, Vol. 122, 2018, pp. 707–718.

[47] Hansman, R. J., and Kirby, M. S., "Comparison of Wet and Dry Growth in Artificial and Flight Icing Conditions," *Journal of Thermophysics and Heat Transfer*, Vol. 1, No. 3, 1987, pp. 215–221. https://doi.org/10.2514/3.30

[48] Shin, J., "Characteristics of Surface Roughness Associated with Leading-Edge Ice Accretion," *Journal of Aircraft*, Vol. 33, No. 2, 1996, pp. 316–321. https://doi.org/10.2514/3.46940